Comparison of Enhanced Resolution Images of Greenland from the ERS-1 and Seasat Scatterometers

David S. Early and David G. Long
Brigham Young University
459 Clyde Building
Provo, UT 84602

Mark R. Drinkwater
Jet Propulsion Laboratory, California Institute of Technology
MS 300-323 4800 Oak Grove Dr.
Pasadena, CA 91109

Abstract - With the increased awareness of the role of ice sheets as a sensitive indicator of global climate change, there is greater need for synoptic interannual studies of major glacial ice masses. Only limited large scale decadal studies of the ice sheets of Antarctica and Greenland have been possible with past and present satellite systems. A recently developed resolution enhancement technique facilitates the use of scatterometer data for extended studies of glacial ice at medium scale resolution with hemispheric or even global coverage possible. In this paper, we compare previously published results for the Seasat-A scatterometer with current ERS-1 scatterometer data for Greenland. Illustrative images and data plots are provided.

I. INTRODUCTION

Increasing interest in the role of ice sheets in regulating global climate has created a need for synoptic interannual recording and monitoring of the earth's major ice sheets. Satellite imaging presented scientists with a mesoscale mapping tool in the early 1970's. Unfortunately, these early systems were mostly visible wavelength systems and were limited in temporal resolution and by weather conditions. The introduction of spaceborne microwave radar with Seasat in 1978 presented a new kind of tool for monitoring global ice conditions to the scientific community that did not suffer from the limitations of visible wavelength systems.

Although microwave radar has increased capabilities over some aspects of visible wavelength systems, there are tradeoffs between spatial and temporal resolution. Synthetic aperture radar (SAR) can make high resolution images, but is limited in ground coverage over polar regions because of high data rates and a lack of receiving stations. Scatterometers are capable of greater ground coverage in polar regions, but are inherently low resolution instruments. However, a recently developed resolution enhancement technique for SASS can increase scatterometer resolution and generate enhanced resolution σ^o images.

In a previously published study, the Greenland ice sheet was studied using the Seasat-A Scatterometer (SASS) and key ice facies were investigated and mapped using simple parametric scattering models (Long and Drinkwater, 1994). The resolution enhancement technique for ERS-1 is described in *Long et al.* (1994). In this paper, we use the resolution enhancement technique to study the Greenland ice sheet with historic Seasat-A scatterometer data (1978) and current data (1992) from the ERS-1 Active Microwave Instrument (AMI) scatterometer. First, we present a time series of images for corresponding time periods from both data sets in which seasonal variations are evident. Second, using simple scattering models, we present preliminary results in mapping the extent of the snow facies at C-band for ERS-1 and compare this to SASS at Ku band and results in *Fahnstock et al.* (1993).

II. GREENLAND IMAGES

SASS made 14.6 GHz measurements of hh- and vv-polarized σ^o on ascending and descending orbits at various azimuth and incidence angles. ERS-1 made 5.3 GHz measurements of vv-polarized σ^o on ascending and descending orbits at various azimuth and incidence angles. Enhanced resolution images can be generated from scatterometer data sets using a new method, and although the method was originally developed for SASS data, simple modifications allow it to be used with ERS-1 data. However, due to differences in data processing, the achievable resolution for ERS-1 is lower than that obtainable for SASS [see Long et al. (1994), Daum et al. (1994)]. The images presented here are at nominally 10km resolution for SASS and nominally 14km resolution for ERS-1. Even with these differences, productive comparison can still be made with the understanding that the resolution of the ERS-1 data is slightly lower than the SASS data.

Since σ^o for glacial ice is a function of incidence angle, we have normalized σ^o to the mean incidence angle of 40° . The relationship of σ^o (in dB) to incidence angle is approximately linear in the range of θ in the data and is given by:

$$10log_{10}\sigma^o(\theta) = \mathcal{A} + \mathcal{B}(\theta - 40^\circ) \qquad (1)$$

In Eq. (1), $\mathcal{A}$ is the 40° "incidence angle-normalized" σ^o , and $\mathcal{B}$ describes the dependence of σ^o on θ. Both vary with surface conditions. By normalizing σ^o in this way, we remove the θ dependence to allow easy comparison of data without the modulation caused by varying incidence angles. The images presented in this paper are for the $\mathcal{A}$ values derived from this relationship.

To achieve the resolution enhancement, multiple orbits are required to provide a sufficient number of overlapping measurements; and several days of data are required. Each SASS image corresponds to an *average* of 14 days of data and ERS-1 images correspond to an *average* of 7 days of ERS-1 data. Over the Greenland ice sheet, conditions are assumed invariant over the 1 to 2 week integration time so that the averaging process does not preclude use of the data for geophysical studies. *Long and Drinkwater* (1994) have investigated the impacts of varying conditions upon the imaging process.

Figure 1 presents a time series of four $\mathcal{A}$ images of Greenland generated from 1978 SASS data with the resolution enhancement technique. Figure 2 is a corresponding time series generated from 1992 ERS-1 data. Although the integration time for the two systems is different, corresponding images from both ERS-1 and SASS data are centered about the same Julian day as indicated.

III. INTERPRETATION AND FACIES MAPPING

To illustrate the variation of $\mathcal{A}$ over time, we plot $\mathcal{A}$ and $\mathcal{B}$ versus Julian day for both the SASS data and the ERS-1 data for a 1° x 1° study region in the ablation zone. The lower left hand corner of the cell is 48° W 66° N. Figure 3(a) is from SASS data and Figure 3(b) is from ERS-1 data. In the upper part of each figure the solid line represents a running ten-day average of the $\mathcal{A}$ value and the dashed line a running ten-day average of the $\mathcal{B}$ value. The actual $\mathcal{A}$ values are plotted on the lower half of the plot with the average $\mathcal{A}$ line superimposed on the scatter plot. The ERS-1 data set is missing data between JD 188 and JD 205. Differences in response can be attributed in part to the different frequencies of each instrument. The Ku-band SASS data is more sensitive to surface melt and snow grain characteristics and the surface roughness scale so snow surface layer and snow/ice interface scattering dominate the backscatter at this frequency. At C-band, the longer wavelength signal penetrates deeper into the surface so subsurface elements such as ice lenses in the percolation zone contribute more to backscatter. Even with these differences, however, the main ice-sheet features are still visible in each image set.

Using a simplified parametric scattering model and *in-situ* measurements for different ice facies characteristics, scattering response is modeled for these different ice facies at Ku-band. This information can then be used to create an ice facies map as shown in Figure 4 for the SASS data (from *Long and Drinkwater* (1994)). When applied to ERS-1 data, however, the model must be more complex to account for the increased participation of volume scattering at C-band.

A. Dry Snow

A parametric modeling exercise, based on the study in Long and Drinkwater (1994) reveals that the C-band scatterometer senses much deeper into the ice sheet surface that was the case for the Ku-band SASS. Typical penetration depths in the dry snow zone are on the order of several meters. In order to simulate the results for the dry snow zone for ERS-1, the same model layer parameters were selected as shown in Fig. 11 of Long and Drinkwater (1994). The result of the volume scattering model should, to a degree, be self-scaling, with the effect of snow grain scattering becoming less effective with an increase in wavelength relative to the size of the Rayleigh scatterers. Thus the same snow grain size and density were used and the snow surface roughness modified to fit the observations. It is found that the C-band is sensitive to layering of the snow, but that the *effective* volume sensed by the penetrating wave is correspondingly larger, with the depth of the snow layer modified to 10m. C-band is also sensitive to slightly

different scales of surface roughness, and the standard deviation and correlation length scales are adjusted slightly. Figure 5 is an sample data fit to the model numbers. Model data is superimposed on the data from a 2° x 2° study area in the dry snow zone with a lower left hand corner at 40° W and 69° N.

Clearly, snow grain volume scattering is unimportant in the dry snow zone given the relatively high value of $\mathcal{B}$ in this area. The model result confirms that the level of volume scattering is below -25dB in this case, where only snow grain scattering contributes to the volume signal. A contrasting situation is observed in a 1° x 2° study region at 40° W and 75° N in dry snow zone I to the north on the ice sheet. The higher backscatter and lower gradient indicate that the scattering characteristics of dry snow zone I are radically different (Long and Drinkwater, 1994). Model simulations in the first study region suggest that layering is much more dominant in signatures from this part of the ice sheet. This implies that the accumulation processes are somewhat different to the north of the ice divide, perhaps due to lower annual precipitation and different wind patterns.

B. Ablation Zone

In the first image of each set, the ablation zone is clearly visible on the western side of the ice sheet as a dark stripe running north-south. Note the difference in the width of the dark stripe between the SASS and ERS-1 images. The wider ablation zone in the SASS data may indicate that there was more liquid present on the ice sheet in 1978 than in 1992. This difference may also be related to the greater penetration at C-band and thus to variations in the up-slope response to ice sheet sub-structure in the border area between the ablation and percolation zones. As the time series moves from late July through late September, the ablation zone refreezes as the season changes from summer to winter. Note that the data from both satellites indicate similar time periods for the refreezing event.

IV. CONCLUSION

Evidently, these enhanced resolution images are capable of monitoring development of ice scattering characteristics over time. Further work is in progress to develop more appropriate scattering models, and thus to improve our ability to monitor interannual changes in ice surface characteristics at C-band.

ACKNOWLEGEMENTS

This work was supported by the National Aeronautics and Space Administration (NASA) under Dr. Robert Thomas. Part of this work was carried out at the Jet Propulsion Laboratory, California Institute of Technology under contract to NASA, with the remainder (DGL and DSE) conducted at Brigham Young University. We thank ESA for the use of the data. MRD carried out this research as one component within the PIPOR Study PIP. Ant3.

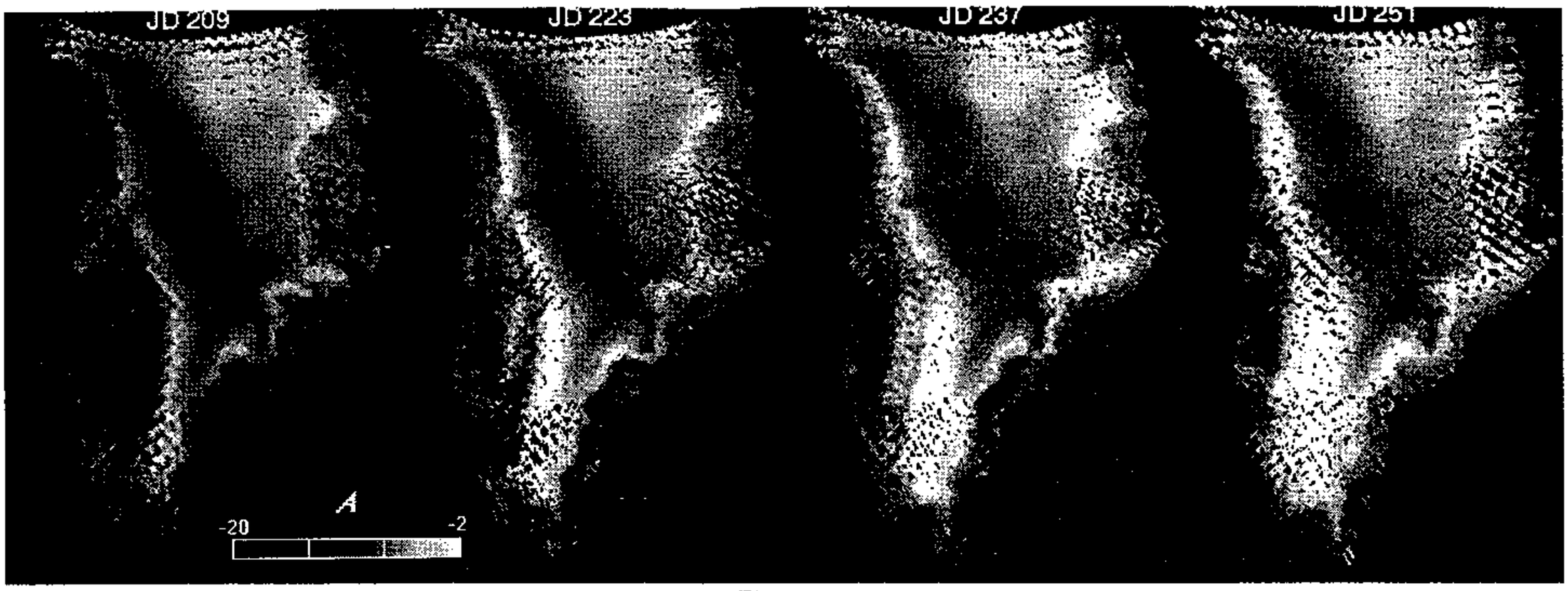

Figure 1
SASS $\mathcal{A}$ images from late July to early September, 1978. Data copyright ESA 1992.

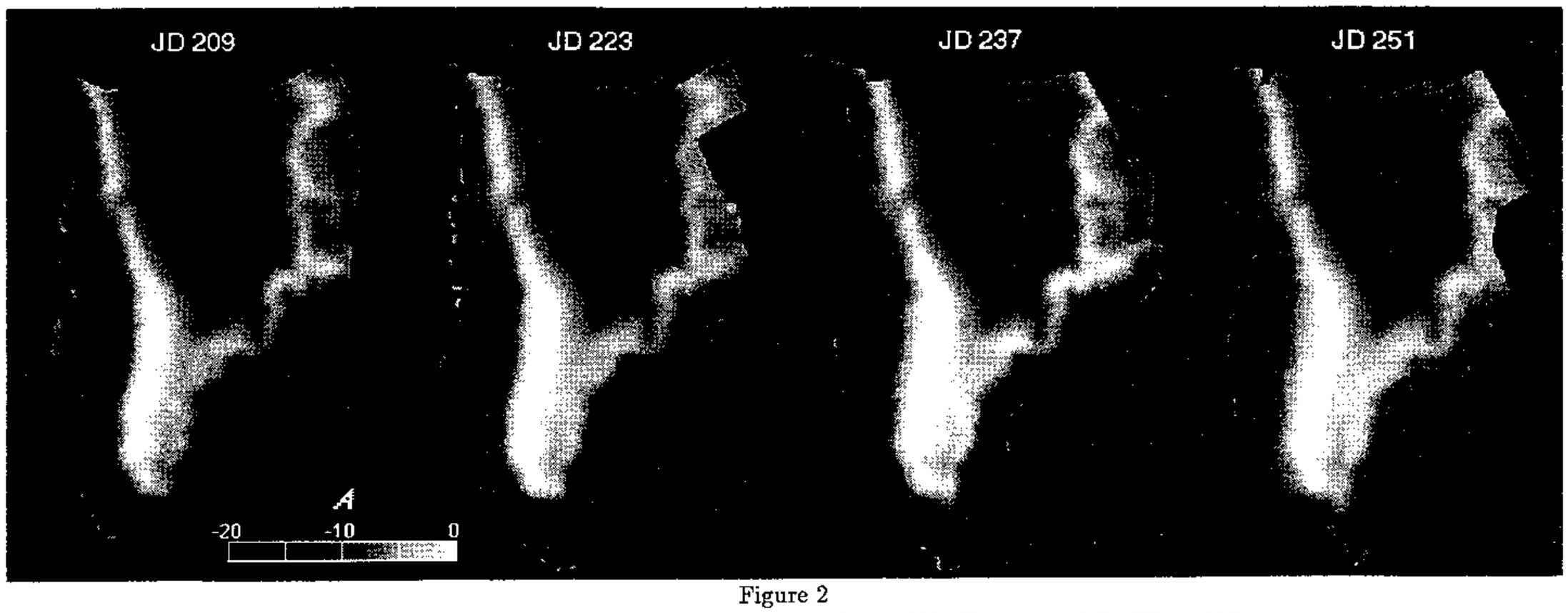

Figure 2
ERS-1 $\mathcal{A}$ images from late July to early September, 1992. Data copyright ESA 1992.

REFERENCES

Daum, D.R., D.G. Long and W.B. Davis, "Reconstructing Enhanced Resolution Images from Spaceborne Microwave Sensors," in IGARSS digest, 1994.

Fahnstock, M., R. Bindschadler, R. Kwok, and K. Jezek, "Greenland Ice Sheet Surface Properties and Dynamics from ERS-1 SAR Imagery," *Science*, Vol. 262, pp. 1530-1534, 1993.

Long, D.G., D.S. Early and M.R. Drinkwater,"Resolution Method," in IGARSS digest, 1994.

Long, D.G. and M.R. Drinkwater, "Greenland Ice Sheet Surface Properties Observed by the Seasat-A Scatterometer at Enhanced Resolution," *J. of Glaciology*, Vol. 135, In Press, 1994.

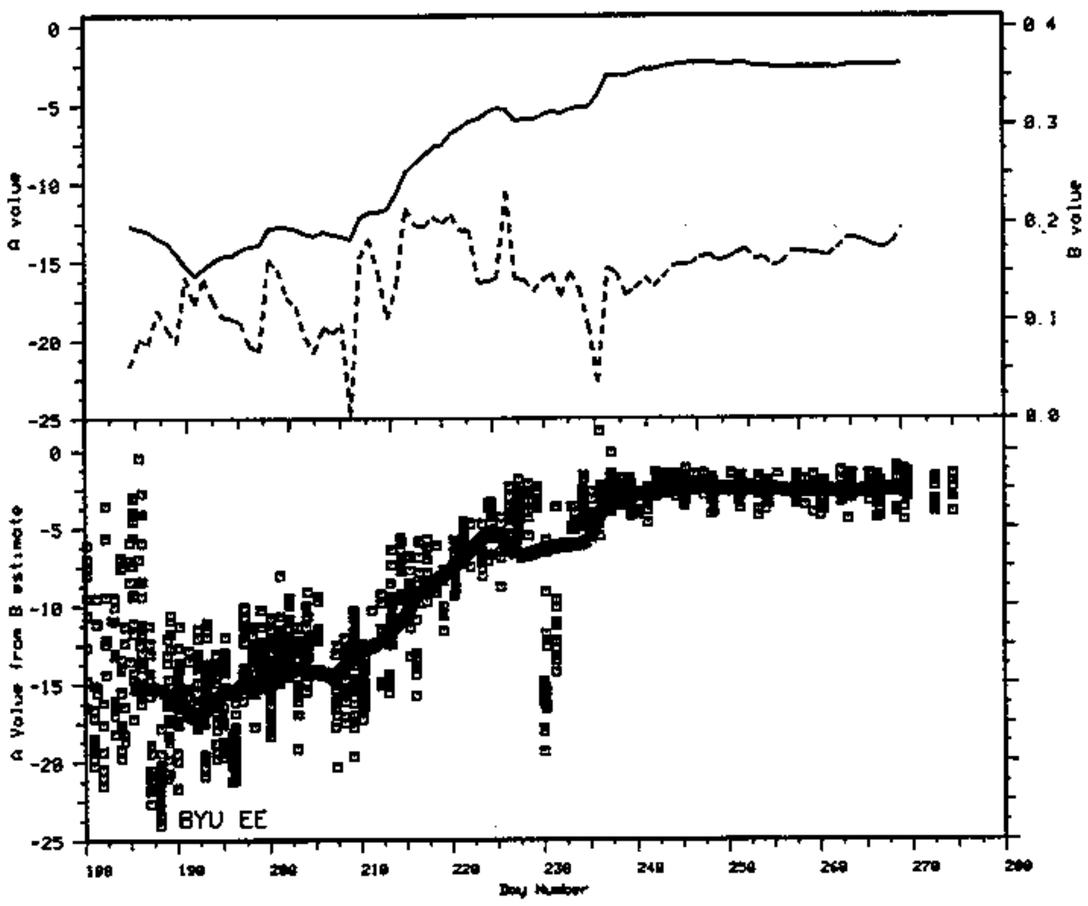

Figure 3(a)
SASS $\mathcal{A}$ values versus time for the 1° x 1° study region in the ablation zone from JD 188 to JD 288 are plotted versus a time scale. Note the greater variation early in the data sets, corresponding to a period of surface melting. As the surface freezes, the response levels out.

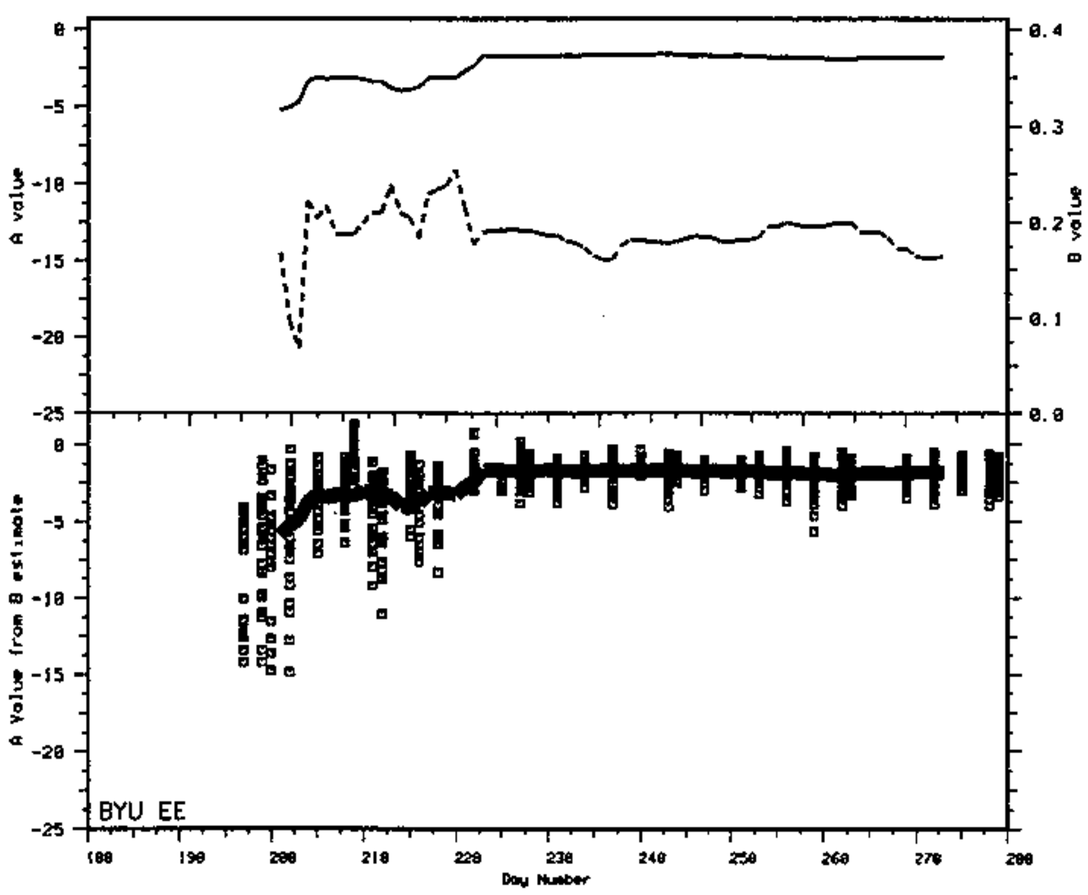

Figure 3(b)
ERS-1 $\mathcal{A}$ values versus time for the same study region as Figure 3(a).

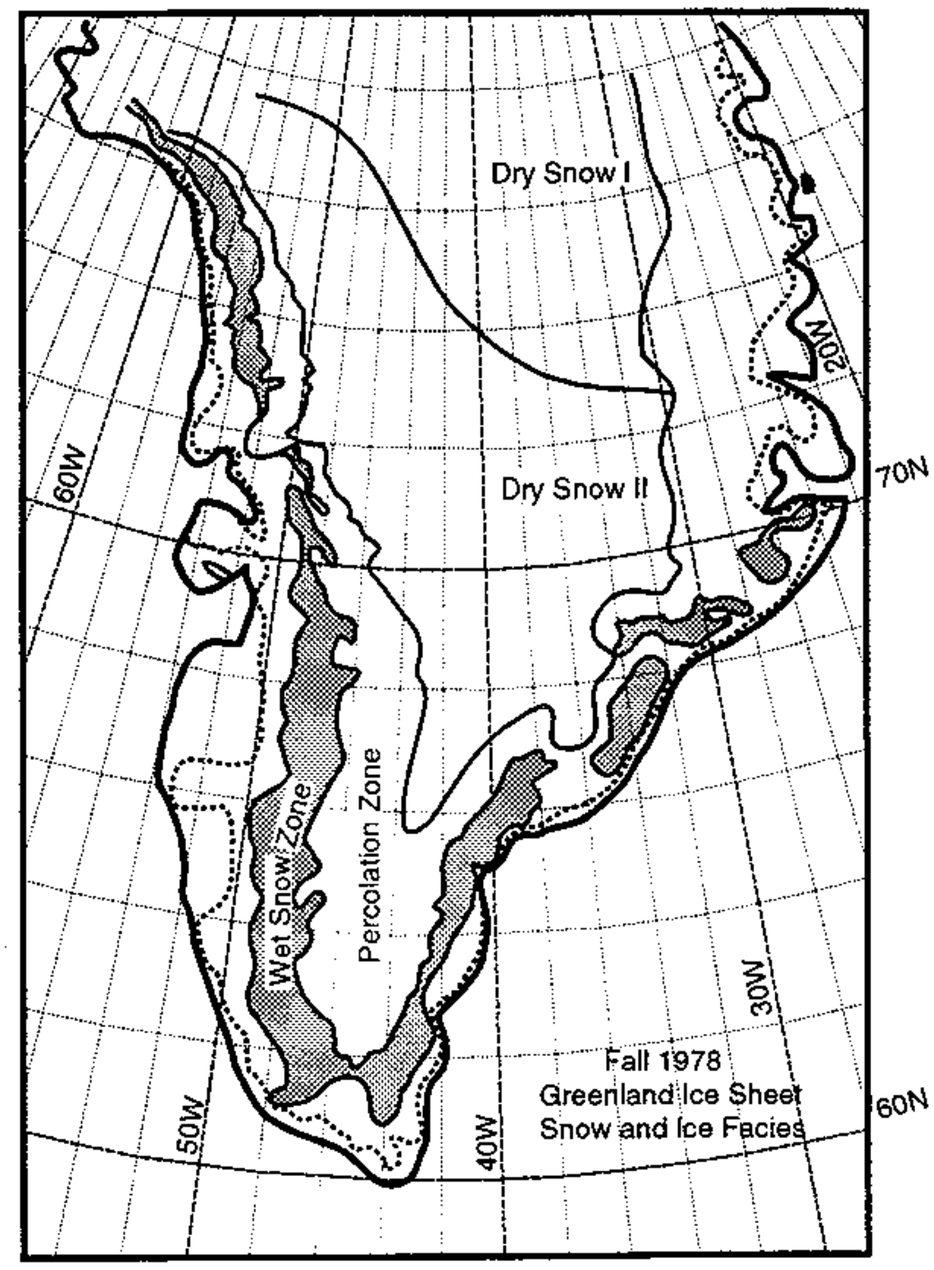

Figure 4
Ice facies map. From *Long and Drinkwater* (1994).

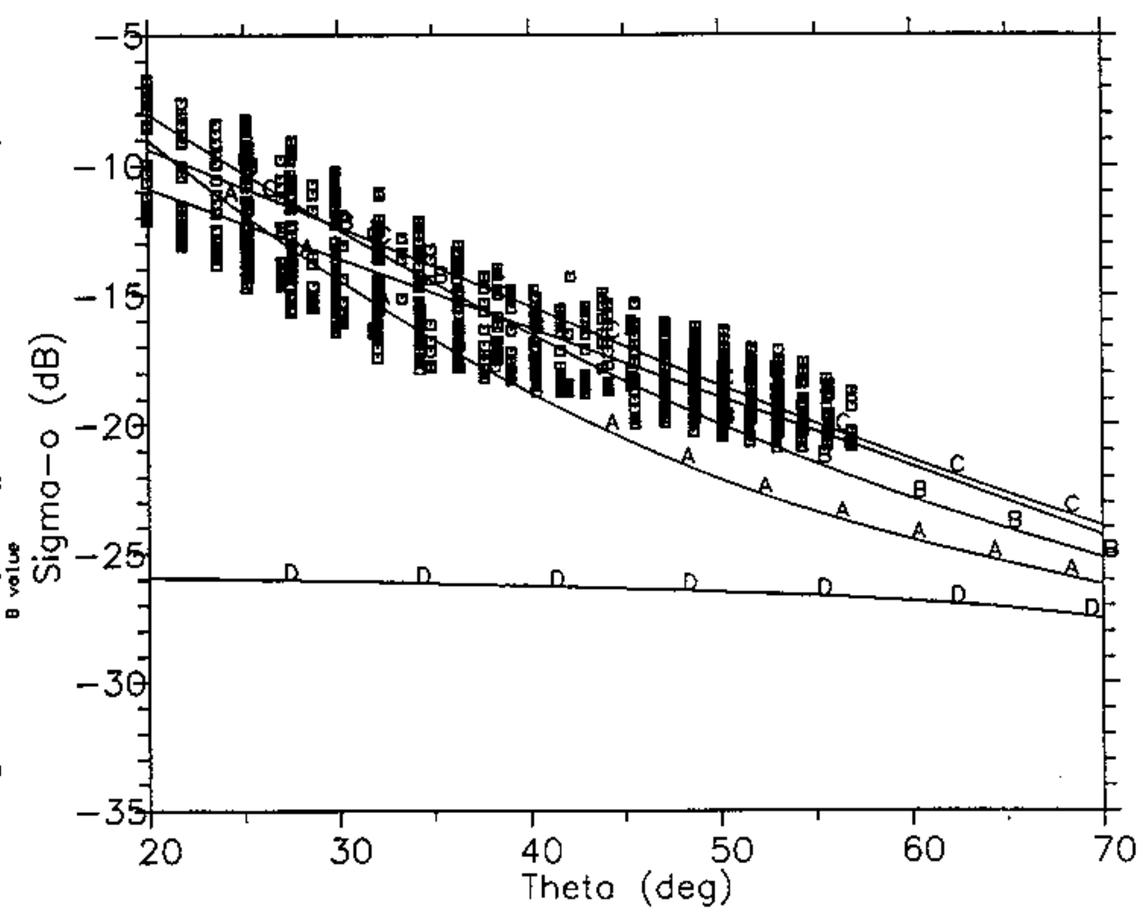

Figure 5
Model results are superimposed over a scatterplot of data from a dry snow zone study region. Note that the data fits well to the C parameters.